Effects of disorder on the current density and recombination profile in organic light-emitting diodes

R. Coehoorn and S. L. M. van Mensfoort
Philips Research Laboratories, High Tech Campus 4, Box WAG-12, 5656 AE Eindhoven, The Netherlands
and Department of Applied Physics, Eindhoven University of Technology, P.O. Box 513, 5600 MB Eindhoven, The Netherlands
(Received 18 January 2009; revised manuscript received 1 May 2009; published 5 August 2009)

In this paper the effects of energetic disorder on the current density and recombination profile of single-layer organic light-emitting diodes (OLEDs) with Gaussian shapes of the electron and hole densities of states are studied. Gaussian disorder is found to give rise to a strong enhancement of the double carrier current density as compared to the sum of the single-carrier current densities and, in symmetric OLEDs, to a strong confinement of the recombination profile to the center of the device. The study is made using a OLED device model which makes use of a one-dimensional master-equation method within which hopping takes place in between discrete sites at physically meaningful intersite distances and within which the intersite hopping rates are consistent with the carrier density dependence of the mobility as obtained by Pasveer *et al.* [Phys. Rev. Lett. **94**, 206601 (2005)]. The model is shown to provide physically transparent descriptions of the dependence of the mobility and the recombination rate on the electric field, based on results from three-dimensional modeling. An outlook is given on applications to multilayer OLEDs.

DOI: 10.1103/PhysRevB.80.085302 PACS number(s): 72.80.Le, 85.60.Jb, 72.20.Jv

I. INTRODUCTION

The functioning of organic light-emitting diodes (OLEDs) as energy efficient and stable light sources[1–3] depends strongly on the shape of the recombination profile, i.e., on the dependence of the recombination rate on the position within the active semiconducting single-layer or multilayer material. For example, the shape of the recombination profile determines the wavelength-dependent light outcoupling efficiency, as a result of microcavity effects such as waveguiding and exciton quenching at the metallic electrodes.[4] In this paper, we focus on OLEDs based on a single organic light-emitting layer. As predicted by Parmenter and Ruppel,[5] the recombination profile is fully uniform across the emitting layer when (i) the electron and hole mobilities and diffusion coefficients are equal and constant, (ii) injection at the contacts is ideal, (iii) the bimolecular recombination rate is described by the Langevin equation,[6] and (iv) the diffusion contribution to the current density is neglected. Neumann *et al.*[7] showed that when the diffusion contribution is taken into account the recombination profile is not anymore fully uniform, but shows a significant decrease in interfacial zones near the electrodes, and vanishes at the electrodes. When, in addition, the electron and hole mobilities are not constant but show a field dependence as described by a Poole-Frenkel factor, the recombination rate shows a local minimum at the device center and two maxima more close to the electrodes.[8]

In the OLED models discussed above the effects of energetic disorder of the localized states in between which the hopping takes place have been neglected. For the case of a Gaussian shape of the density of states (DOS), it has recently been shown that the mobility is not only dependent on the temperature and the electric field[9] but also on the charge-carrier density. This effect depends on the ratio of the width of the Gaussian DOS, σ, and the thermal energy, k_BT, with k_B the Boltzmann constant and T the temperature.[10–12] We will refer to the parametrization of the temperature, field, and density-dependent mobility as given by Pasveer *et al.*,[11] based on the results of a master-equation (ME) study, as the "extended Gaussian disorder model" (EGDM). Successful quantitative descriptions of hole transport in *para*-phenylene-vinylene and polyfluorene-based sandwich-type devices, assuming a Gaussian DOS, were given by Pasveer *et al.*[11] and Van Mensfoort *et al.*,[13] respectively.

In this paper, we investigate the effects of Gaussian disorder on the current density and recombination profile in single-layer OLEDs. In principle, it would be possible to investigate these effects by introducing the EGDM in one of the one-dimensional (1D) OLED device models which are already available.[14–25] However, it is presently not clear to what extent the true 3D character of the filamentary transport[26] and recombination processes can be described using a 1D model. More specifically, it is presently not yet clear to what extent bimolecular recombination in materials with Gaussian disorder is properly treated using the Langevin formula. Albrecht and Bässler[27] studied the recombination rate in the independent particle (Boltzmann) limit using three-dimensional (3D) Monte Carlo (MC) calculations, and found (i) at small fields no significant deviation from the Langevin rate when varying the disorder parameter σ and (ii) a significant enhancement of the recombination rate with respect to the Langevin rate with increasing field. In contrast, Groves and Greenham[28] recently found from a MC study that in homogeneous systems (a box with periodic boundary conditions) with isotropic mobilities the bimolecular recombination rate can be larger than given by the Langevin formula when $\sigma \gg k_BT$. So far, no systematic study of the charge-carrier density dependence of the recombination rate has been performed.

It may be envisaged that true future benchmark OLED device models will be based on MC simulations of the transport and recombination as resulting from 3D hopping processes in between discrete sites, with proper injection boundary conditions at the electrode planes. Thereby, any possible

arbitrariness concerning the injection of new particles is avoided. Such calculations are inevitably computationally rather expensive, so that 1D continuum models will remain of interest as a practical tool for analyzing the measured properties of OLEDs and for exploring the potential of novel OLED device structures. It will thus be of importance to "translate" the results of 3D modeling to effective 1D models.

In order to facilitate such a 3D-1D translation step, we develop in the first part of this paper (Sec. II) a OLED device model which may be viewed as intermediate in between 3D (discrete) and 1D (continuum) models. Within the model, the discreteness of the sites, positioned at physically meaningful intersite distances, is retained, but the transport is treated as one-dimensional. A ME method is used for solving the drift-diffusion-recombination problem. The method is constructed such that the intersite hopping rates at zero field are consistent with the carrier density dependence of the mobility, as obtained within the EGDM. We show how the model predicts in a natural way why the field dependence of the recombination rate is expected to be larger than as given by the Langevin formula and how thermal electron-hole pair generation should be modeled. It is also shown that the model provides a physically transparent and quantitatively accurate description of the field dependence of the mobility. Previously, the field dependence of the mobility as obtained within the EGDM was only described in a phenomenological way.

In the second part of the paper (Sec. III), the model is applied to single-layer OLEDs with equal electron and hole mobilities ("symmetric OLEDs") and with unequal mobilities ("asymmetric OLEDs"). It is found that (i) the current density is unexpectedly large as compared to that in otherwise identical single-carrier devices and (ii) in symmetric OLEDs the recombination profile becomes with increasing disorder more confined to the device center, as a result of the carrier density dependence of the mobility. Section IV gives a summary and an outlook on extensions of the model, including applications to transport across organic-organic interfaces in multilayer OLEDs.

II. OLED DEVICE MODEL

Within the OLED device model developed in this section, transport is described as resulting from nearest-neighbor hopping along linear chains of discrete electron and hole sites, shown in Fig. 1(a), with site indices $i=0$ (anode) to N (cathode). The distance between the sites is equal to ζa, with a the average intersite distance in the organic semiconductor and ζ a number of order unity. The average carrier concentration at each site is determined self-consistently using a 1D-ME approach within which it is required that for electrons and holes the total rate of hops toward each site is equal to the sum of the total rate of hops away from that site and the recombination rate at that site. The hop rates are derived from a two-level model, and are chosen such that at zero electric field the resulting carrier-concentration-dependent mobility is fully consistent with the EGDM. We find that the lattice parameter ζa can be taken such that the electric field dependence of the mobility is in good agreement with the EGDM. The model includes the correct carrier density and electric field dependence of the diffusion coefficient in an implicit manner, and is fully consistent with the principle of detailed balance.

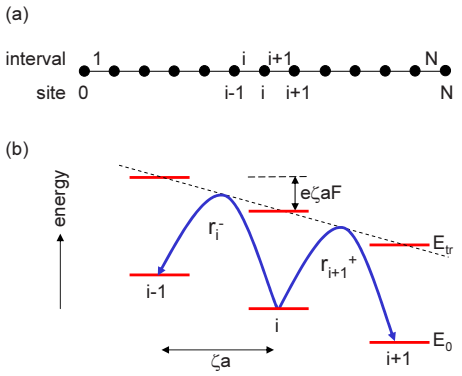

FIG. 1. (Color online) (a) The linear chain of discrete sites, assumed within the 1D-ME model; (b) Schematic view of the hopping process between sites at energy levels E_0. The figure shows the special case in which the electrostatic field is uniform (linear variation in the transport energy, E_{tr}, with position) and in which the carrier density is uniform (so that the activation energy, $E_{tr}-E_0$, is uniform).

A. Single-carrier transport

In the case of single-carrier transport the net current density from site $i-1$ to i across interval i, is assumed to be given by

$$J_i = (c_{i-1}r_i^+ - c_i r_i^-)\frac{e}{a^2}, \tag{1}$$

with c_i the carrier concentration (occupation probability) on site i, $r_i^{+(-)}$ the forward (backward) hopping rates across interval i, and e the elementary charge. We consider a Gaussian DOS with width σ and define a dimensionless disorder parameter $\hat{\sigma} \equiv \sigma/(k_B T)$. In order to obtain an expression for the hopping rates, we make a transformation of the numerically exact 3D master-equation results obtained in Ref. 11 to the 1D system defined above. Use is made of the "transport level" concept.[9,29] At zero electric field, the forward and backward hopping rates are determined by a local thermal activation energy, $E_A(n) \equiv E_{tr} - E_0(n)$, which is equal to the energy difference between (i) an effective transport level, E_{tr}, which is in most cases of interest situated close to the center of the DOS and (ii) a characteristic starting energy, E_0, which depends on the local carrier density, n, and which is usually situated in the tail of the DOS. In Ref. 30, it was already shown that the carrier density dependence of the mobility can be understood well from the transport level concept. Below, we show that the concept also provides a good description of the electric field dependence of the mobility.

For very small carrier densities, in the Boltzmann regime, the carriers act like independent particles. The mobility in this regime, μ_0, is independent of the carrier density. For carrier densities above a critical value, $n_{cr} = (1/2)a^{-3}\exp(-\hat{\sigma}^2/2)$,[30] E_0 increases with increasing den-

sity, so that the activation energy decreases. This results in a density- and disorder-dependent enhancement, $g(n,\hat{\sigma})$, of the hopping rates, and hence of the mobility, with respect to the values in the Boltzmann limit. At zero field and at small carrier densities, E_{tr} is to excellent approximation independent of the carrier density, leading to a simple analytical expression for $g(n,\hat{\sigma})$ [Eq. (28) in Ref. 30]. However, for relatively large carrier densities, this approach would overestimate the actual mobility. First, the increase in E_{tr} with increasing density is then not quite negligible and second, the finite probability that the final state is already occupied reduces the mobility. In this paper, both effects are to a good approximation taken into account by describing $g(n,\hat{\sigma})$ as given in Appendix A.

The presence of an electrostatic field, F, decreases and increases the effective thermal activation barrier for downstream and upstream hops, respectively. We position the effective barrier halfway between each pair of sites [see Fig. 1(b)], and use the following expression for the hopping rates across interval i:

$$r_i^+ = g(n_{i-1},\hat{\sigma}_{i-1})\exp\left(+\frac{e\zeta aF_i}{2k_BT}\right)\times r_{0,i-1} \tag{2}$$

and

$$r_i^- = g(n_i,\hat{\sigma}_i)\exp\left(-\frac{e\zeta aF_i}{2k_BT}\right)\times r_{0,i}, \tag{3}$$

with $n_i=c_i/(\zeta a^3)$ the carrier density and with [from Eqs. (1)–(3)]

$$r_{0,i} = \frac{\mu_{0,i}k_BT}{\zeta^2 a^2 e} \tag{4}$$

the hopping rate in the zero density and zero-field limit. The latter quantity is site dependent in the case of transport in a layered structure.

By considering the current density in a system with a uniform carrier density (no diffusion), it follows straightforwardly from Eqs. (1)–(4) that the mobility may be expressed as a product of a density-dependent and field-dependent factor: $\mu(n,T,F)=g(n,\hat{\sigma})\times f(F)\times\mu_0$. Defining $\hat{F}\equiv\zeta aeF/(2k_BT)$, it follows that the field dependence is given by

$$f(F) = \frac{\sinh\hat{F}}{\hat{F}}, \tag{5}$$

with $f(0)=1$. The model thus provides an explanation for the empirical finding obtained from the 3D-ME calculations in Ref. 11 that the mobility in a Gaussian DOS may be factorized. Making use of the density and temperature dependence of the mobility obtained in Ref. 11 (EGDM), the full expression for the mobility as obtained in the 1D-ME model is given by

$$\mu_{1\mathrm{D}}(n,F,\hat{\sigma}) = g(n,\hat{\sigma})f(F)\exp(-C_2\hat{\sigma}^2)\times\mu^*, \tag{6}$$

with $\mu^*\equiv C_1a^2\nu_0e/\sigma$, where ν_0 is the hopping attempt frequency and where $C_1=1.8\times10^{-9}$ and $C_2=0.42$ are fit parameters. C_1 is very close to the overlap between the localized wave functions in between which the hopping takes place, $\exp(-2\alpha a)$, where α is the inverse of the wave-function extension. In Ref. 11, α^{-1} is taken to be equal to a tenth of the intersite distance, so that $\exp(-2\alpha a)=\exp(-20)=2.06\times10^{-9}$. In the remainder of this paper we will neglect the small difference.

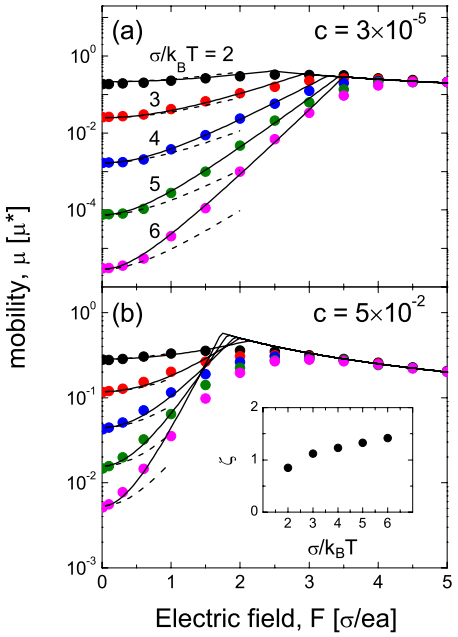

FIG. 2. (Color online) Electric field dependence of the mobility, in units μ^*, at various values of the disorder parameter σ/k_BT, as obtained in Ref. 32 from 3D-ME calculations (symbols), and as obtained from the 1D-ME method introduced in this paper using a disorder-dependent intersite distance ζa (full curves) and using the actual intersite distance a (dashed curves). Figures (a) and (b) give the results for carrier concentrations $c=3\times10^{-5}$ and 5×10^{-2}, respectively. The inset in figure (b) shows the σ/k_BT dependence of the ratio ζ. The mobility enhancement functions $g(c,\hat{\sigma})$ are taken equal to the values obtained from the 3D results, so that the figures show (by definition) exact agreement for $F=0$.

In the Boltzmann regime, the correct value of the diffusion coefficient, $D_0=(k_BT/e)\mu_0$ (Einstein equation) is obtained. Outside the Boltzmann regime, the approach is consistent with the generalized Einstein equation,[31] provided that the model is understood to describe transport in an effective DOS with a shape that is almost but not precisely Gaussian. This is shown and further discussed in Appendix A, using the principle of detailed balance.

The parameter ζ is chosen such that the function $f(F)$ most optimally describes the field dependence of the mobility as obtained from 3D-ME calculations. In Fig. 2 a comparison is given between the field-dependent mobility as obtained using the 3D-ME method (symbols, data taken from Ref. 32) and the mobility as obtained using the 1D-ME model using $\zeta=1$ (dashed curves) and using an optimized value of ζ (full curves). The comparison is made for various values of $\hat{\sigma}$ and for relatively small and relatively large carrier densities [Figs 2(a) and 2(b), respectively]. For $\zeta=1$ and for small $\hat{\sigma}$, fair agreement is observed between the dashed curves and the 3D-ME results. However, for values $\hat{\sigma}$ around and above 4 the field dependence is underestimated. Using

optimized values of ζ (full curves) leads, for small fields, to excellent agreement with the 3D-ME results. The values of ζ vary from approximately 0.8 to approximately 1.4 for $\hat{\sigma}$ varying from 2 to 6, as shown in the inset in Fig. 2(b). The increase in ζ with increasing $\hat{\sigma}$ may be understood as a consequence of an increase in the effective hopping distance with increasing disorder, from nearest-neighbor hopping for small $\hat{\sigma}$ to variable range hopping for large $\hat{\sigma}$, as is well known from percolation theory (see, e.g., Figure 6 in Ref. 30).

At high fields a different transport regime sets in. In the actual 3D system this happens when the energy of most downstream nearest-neighbor states is lower than the energy of the initial state, so that the mobility-determining hops are no longer thermally activated.[11] Within our model, the crossover is defined to take place at the field for which the effective thermal activation energy for forward hops becomes negative. The extension of the model to this regime is discussed in Appendix B. As shown in Fig. 2, the field at which the transition to this regime takes place is well described by the model, although for the highest of the two concentrations considered, $c=5\times10^{-2}$, the actual transition is actually somewhat less abrupt than as predicted.

The model can applied to the general case of injection across a finite injection barrier, leading to a reduced carrier density at the electrode planes. The following iterative procedure is then used for obtaining self-consistent values of the carrier concentrations and electric fields at each site and interval, respectively, from which the current density is calculated. First, a trial carrier concentration distribution across the device is chosen. Second, the field distribution is calculated using the Poisson equation, assuming the presence of $N-1$ laterally uniform charge-density sheets with infinitesimal thicknesses, assuming that the electrodes are perfect conductors, and taking the field due to the applied voltage, V/L, into account. Third, a new c value is calculated at each site i by requiring *local* dynamic equilibrium, i.e., by requiring that $J_i=J_{i+1}$. Subsequently, the last two steps are repeated until the current densities across all intervals are equal. Our practical implementation of this approach is found to be computationally efficient and stable.

In the case studies presented in Sec. III, we focus on situations without injection barrier, i.e., alignment of the center of the Gaussian DOS with the Fermi level in the electrodes so that $n_0=n_N=1/(2a^3)$. This boundary condition provides at present the best possible model treatment of the case with "ideal Ohmic contacts." Although it is arguable whether the EGDM would adequately describe the transport at such high carrier concentrations, the conductivity in the contact region is then very large, so that experiments do not sensitively probe this. The zone within which the carrier concentration is larger than 10% is very thin, and already very close to the injecting contacts the carrier density is a few orders of magnitude smaller. The effects of an injection barrier may be included by using as a boundary condition the carrier densities that follows from the condition of thermal equilibrium between the metallic electrode and the organic layer at the interface, as has recently been validated by van der Holst *et al.*[33] using a 3D-ME study. The relationship between the injection barrier and the carrier density is obtained in a manner described in Appendix A.

In order to investigate the precision of the model, we have made a comparison with the current-density versus voltage $[J(V)]$ curves for single-layer single-carrier devices with varying $\hat{\sigma}$ using the continuum 1D drift-diffusion device model presented recently in Ref. 34. For typical devices, such as studied in Fig. 9 of Ref. 34, the agreement is found to be very good. The continuum model presented in Ref. 34 is in practice preferred for single-carrier and single-layer studies, in view of its higher computational efficiency. However, the 1D-ME model presented here is more versatile, as it allows for taking double-carrier transport and complex layer structures (see the outlook in Sec. IV) into account.

B. Double-carrier transport—recombination and generation

In the case of double-carrier transport, the method proceeds in basically the same way as described above, with two adaptations. First, the space charge is calculated from the *net* concentration of electron and hole charges. Second, the relationship between the hole and electron current densities in consecutive intervals is now given by

$$J_{h(e),i}=J_{h(e),i-1}\mp\zeta ae(R_i-G_i), \tag{7}$$

with R_i and G_i the charge-carrier recombination and generation rates per volume unit at site i, respectively (in units s^{-1} m^{-3}). In this subsection, we develop expressions for both rates. For simplicity, we discuss here only situations in which the disorder parameters and intersite distances for holes and electrons are equal.

As discussed in the introduction, it is not well established to what extent in systems with Gaussian disorder the Langevin formula appropriately describes the recombination rate. One of the issues is that it is not *a priori* clear whether the field-dependent mobility functions should be used.[35] Within the derivation of the Langevin formula (see, e.g., Ref. 6), the presence of an external field is not taken into account. The 1D-ME model developed in this paper allows us to deal with this problem in a quite natural way, viz., by assuming that the recombination rate is proportional to the total rate at which as a result of hops to the site considered a carrier meets at that site another carrier of the opposite polarity. When only hops in between sites on a cubic grid are considered, contributions due to hops from three types of nearest-neighbor sites may be distinguished: one upstream site, one downstream site, and four (equivalent) laterally positioned sites. The hop rates from these sites to the central site are dependent on the local field, and proportional to $\exp(\hat{F})$, $\exp(-\hat{F})$ and 1, respectively, for a reduced field $\hat{F}\equiv e\zeta aF/(2k_BT)<\hat{F}^*$. See Appendix B for the case $F>F^*$. We consider the total weight of hops from the lateral sites as a presently unknown parameter, k, to be deduced from 3D Monte Carlo calculations. The field dependence of R is then equal to

$$h_k(\hat{F})=\frac{1}{2+k}[\exp(\hat{F})+\exp(-\hat{F})+k]. \tag{8}$$

The upper part of Fig. 3 shows, as an example, schematically the recombination process assumed when taking $k=0$ (recombination only due to longitudinal hops) or $k=4$. The

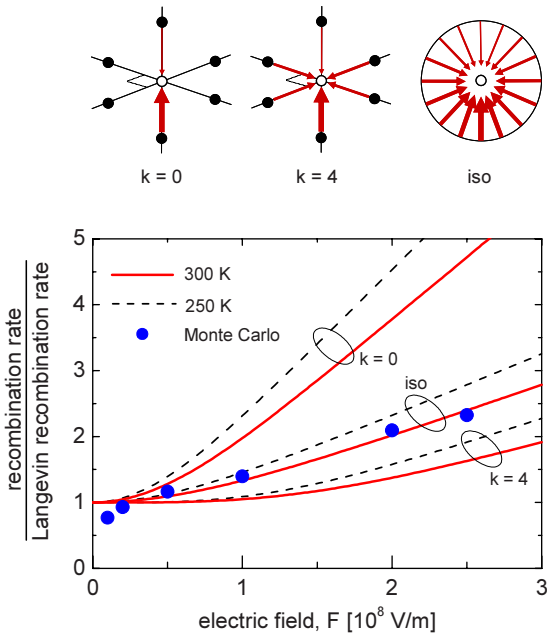

FIG. 3. (Color online) Ratio of the actual and Langevin recombination rates for a system with a Gaussian DOS with $\sigma=0.1$ eV and $a=0.8$ nm. The full and dashed curves give the functions h_0/f, h_4/f, and $h_{\rm iso}/f_{\rm iso}$ at 300 K and 250 K, respectively, corresponding to recombination processes as shown schematically in the top part of the figure. The closed circles (with $a\pm0.3$ uncertainty at the two lowest fields) give averages of 250 K and 350 K results obtained in Ref. 27 from MC calculations. These calculations revealed no significant temperature dependence.

lower part of Fig. 3 gives for the cases $k=0$ and 4 the ratio $h_k(F)/f(F)$ as a function of the electric field at 250 K and 300 K, with $f(F)$ the field dependence of the mobility as given by Eq. (5). The figure shows that the actual field dependence of the recombination rate is larger than the field dependence that would be expected from the Langevin formula, which would predict that $R\propto f(\hat{F})$. Due to the large contribution from field-independent lateral hops, the field dependence of $h_{\rm k}/f$ is for $k=4$ much smaller than for $k=0$.

The prediction from the model given above that the field dependence of the recombination rate is larger than as expected from the Langevin formula is consistent with the findings from a MC study by Albrecht and Bässler.[27] The authors calculated the field dependence of the ratio of the recombination rate and the mobility for a system with Gaussian disorder with $\sigma=0.1$ eV and $a=0.8$ nm, in the low density (Boltzmann) regime. The results, obtained for 250 K and 350 K, are included in Fig. 3 as closed spheres. At 300 K, the field dependence is close to that predicted when taking $k=2$ (not shown). However, no temperature dependence was found from the MC calculations.

The finding that taking $k=2$ provides a good description of the MC results at room temperature is consistent with a more refined "isotropic" approach, within which hops from nearest-neighbor sites which reside uniformly on a sphere are considered. Taking the weight of each contribution equal to $\exp(\hat{F}\cos\theta)$, where θ is the angle between the direction from a nearest neighbor to the central site and the field direction, the field dependence of the mobility and the recombination-rate functions are then given by

$$f_{\rm iso}(\hat{F}) = \frac{3}{2}\int_0^\pi \exp(\hat{F}\cos\theta)\sin\theta\cos\theta d\theta$$

$$= 3\frac{\hat{F}\cosh(\hat{F}) - \sinh(\hat{F})}{\hat{F}^3} \tag{9a}$$

and

$$h_{\rm iso}(\hat{F}) = \frac{1}{2}\int_0^\pi \exp(\hat{F}\cos\theta)\sin\theta d\theta = \frac{\sinh(\hat{F})}{\hat{F}}. \tag{9b}$$

The $\cos(\theta)$ weight factor under the integral in Eq. (9a) takes the angular dependence of the projected hop distance into account. The field dependence of the mobility is smaller than as given by Eq. (5), as the projected hop distances are on average smaller than ζa. Therefore, the function $f_{\rm iso}$, given by Eq. (9a), is inconsistent with the 3D-ME data. We find that it would be possible to solve this issue by an enhancement of the lattice parameter by a factor $\eta=1.27$, making use of the fact that in the field range studied in Fig. 3 to an excellent approximation $f_{\rm iso}(\eta\hat{F})\cong f(\hat{F})$. Figure 3 shows the $h_{\rm iso}(F)/f_{\rm iso}(F)$ ratio which has been calculated including this lattice parameter correction. We find that for the field range considered $h_{\rm iso}/f_{\rm iso}$ is well approximated by h_2/f (not shown).

The MC results given in Ref. 27 suggest that in the Boltzmann limit and for small fields, the recombination rate is well described by the Langevin formula, independent of the disorder parameter. Using the expressions for the hop rates given by Eqs. (2) and (3) or Eqs. (B6), depending on the electric field, the recombination rate at each site (with a volume $V=\zeta a^3$) is then given by

$$r_{rec,i} = \frac{\zeta e^2}{\varepsilon a k_B T} c_{h,i} c_{e,i} [g_h(n_{h,i},\hat{\sigma}_i) r_{0,i,h} + g_e(n_{e,i},\hat{\sigma}_i) r_{0,i,e}] h_k(\hat{F}_i). \tag{10}$$

In view of the uncertainty with respect to the temperature dependence of the recombination rate, it is at present not yet possible to give a final conclusion about the best method for translating results from three-dimensional modeling to the 1D-ME model. In Sec. III, a comparison will be made between the recombination profiles obtained using $k=4$ (the Langevin formula is then an excellent approximation up to fields as high as $\sim10^8$ V/m), and as obtained using $k=2$.

Under conditions of near equilibrium the proper inclusion of a charge-carrier generation term is important. In thermal equilibrium there is no net emission, so the generation rate is then precisely equal to the recombination rate. Near equilibrium occurs at very small voltages, and (at any voltage) close to the metallic electrodes. As far as we know, this issue has not yet been discussed in the literature for the case of disordered organic semiconductors. We assume that the generation rate at each site (with a volume $V=\zeta a^3$) is given by an expression analogous to Eq. (10),

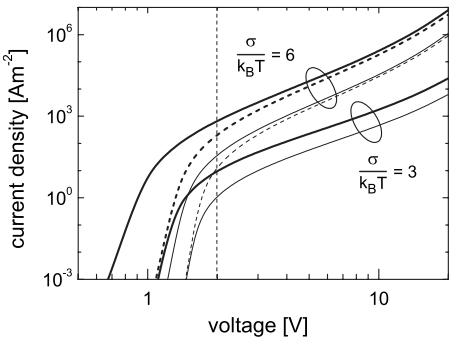

FIG. 4. $J(V)$ curves for transport in symmetric double-carrier (thick curves) and single-carrier (thin curves) devices without injection barriers (solid curves) and with a 0.2 eV injection barrier (dashed, for $\hat{\sigma}=6$ only), based on semiconductors with a Gaussian DOS with equal electron and hole mobilities, with $\mu_0=1\times10^{-10}$ m^2/(Vs) and $\hat{\sigma}=3$ and 6. The other parameters used are: $L=100$ nm, $a=1$ nm, $E_g=eV_{bi}=2$ eV, $\varepsilon_r=3$ (relative dielectric permittivity), and $T=298$ K. The dashed line indicates the built-in voltage.

$$r_{gen,i}=\frac{\zeta e^2}{\varepsilon a k_B T}c_{h,\mathrm{intr},i}c_{e,\mathrm{intr},i}[g_h(n_{h,\mathrm{intr},i}\hat{\sigma}_i)r_{0,i,h}+g_e(n_{e,\mathrm{intr},i},\hat{\sigma}_i)r_{0,i,e}]h_k(\hat{F}_i). \quad (11)$$

Here $c_{\mathrm{h,intr,i}}$ and $c_{\mathrm{e,intr,i}}$ are the intrinsic hole and electron concentrations on site i, respectively, which are obtained by setting the quasi-Fermi levels for electrons and holes equal under the constraint that the charge density is equal to the value $e(n_{\mathrm{h,i}}-n_{\mathrm{e,i}})$ at the site considered. The (R_i-G_i) term in Eq. (7) then properly vanishes at thermal equilibrium.

III. SINGLE-LAYER OLEDS

A. Symmetric OLEDs

We first study the effect of Gaussian disorder on the current density and recombination profile in single-layer 100 nm OLEDs, based on a semiconductor with equal widths of the electron and hole DOS and with equal values of the mobility at zero density and zero field. At the anode and cathode, perfect alignment of the Fermi level with the centers of the hole and electron Gaussian DOSs, respectively, is assumed. In view of the equivalent roles of electrons and holes, we call these devices "symmetric." The energy gap between the highest occupied molecular orbital (HOMO) and lowest unoccupied molecular orbital (LUMO) states, defined as the energy distance between the centers of the densities of states, is taken equal to $E_g=2$ eV. The built-in voltage, V_{bi}, is therefore equal to 2 V. Figure 4 shows the $J(V)$ characteristics for single-carrier and double-carrier devices with $\hat{\sigma}$ equal to 3 and 6. All parameters used are included in the figure caption.

For single-carrier devices it was already shown in Ref. 34 (Fig. 9) that the diffusion contribution to the current density below $V=V_{bi}$ becomes more pronounced with increasing disorder. Figure 4 shows that this effect is even stronger for double-carrier devices. The onset of the current density (and of the light emission) occurs well below the built-in voltage. The current density becomes ohmic (linear in V) at small voltages, outside the range displayed in Fig. 4. The diffusion current density can be reduced by the introduction of an injection barrier, leading to a strong decrease in the current density below V_{bi}. This may be seen from the dashed curves in Fig. 4 for devices with $\hat{\sigma}$ and with a 0.2 eV injection barrier at both interfaces (while keeping V_{bi} equal to 2 V). The resulting hole (electron) carrier concentration at the anode (cathode) interface is then 0.016 carriers per site.

At voltages well above V_{bi}, where the diffusion contribution to the current density is only minor, the current density in double-carrier devices with large disorder is still strongly enhanced as compared to the single-carrier current density. At 10 V, the enhancement is equal to a factor ~7.5 and ~3.8 for $\hat{\sigma}$ equal to 6 and 3, respectively, for the devices studied. The enhancement is only slightly affected when the carrier density at the injecting interfaces is reduced by more than one order of magnitude (dashed curves in Fig. 4). For $\hat{\sigma}=3$, a similarly small effect of introducing a decreased carrier concentration at the interface was found.

Within a drift-only device model which assumes Langevin recombination, the enhancement factor is for symmetric devices with ideal injecting contacts equal to ~2.88.[5] The double-carrier current is larger than twice the single-carrier current due to the partial canceling of the electron and hole space charge in the device. This may be understood in more detail by focusing on the current density in the device center, $J=e\mu_0 n_c F_c$ (per charge carrier), where n_c and F_c are the carrier density and the electric field in the device center. We find that n_c and F_c are enhanced as compared to their values in otherwise equal single-carrier devices by an equal factor, $q=16/(3\pi\sqrt{2})\approx1.20$, consistent with the total enhancement $2\times q^2=256/(9\pi^2)\approx2.88$.[36] Use was made of an analysis given in Ref. 36 for obtaining the position dependence of the density and the field.

The same method is used for analyzing the enhancement for devices with $\hat{\sigma}=6$, at 10 V. The drift contribution to the current density in the device center is given by $J=e\mu_0 g(n_c)f(F_c)n_c F_c$ (per charge carrier), where the g and f functions are the enhancement of the mobility with the density and the field, defined in Sec. II. For the double-carrier device $g(n_c)$, $f(F_c)$, n_c, and F_c are found to be all approximately a factor 1.35 larger than for the single device, explaining a total enhancement factor ~6.6. The remaining difference with the actual factor of ~7.5 is due to the contribution of the diffusion current density. The effect of disorder on n_c is due to a subtle interplay between various effects, as may be seen for the case of single-carrier devices from Fig. 4 in Ref. 34; disorder leads to a larger or smaller value of n_c, depending on the applied voltage.

The effect of Gaussian disorder on the recombination profile is shown in Fig. 5, for $V=3$ and 10 V. The horizontal axis gives the normalized distance to the anode, x/L, and the vertical axis gives the normalized recombination rate, defined such that the integral over the normalized device thickness is equal to 1. For all cases shown, the recombination efficiency, obtained from the ratio of the number of excitons created per charge carrier, was found to be equal to 100 percent. The thick curves show the recombination rate for the case of a constant mobility and diffusion coefficient. They

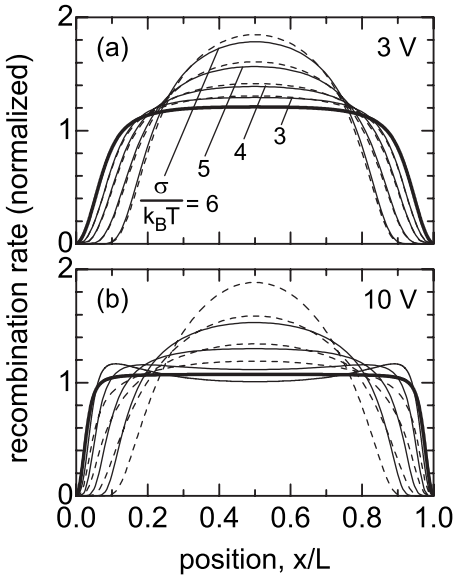

FIG. 5. Position dependence of the normalized recombination density in symmetric 100 nm OLEDs with a Gaussian electron and hole density of states with various values of $\hat{\sigma}$ (thin curves), for the parameter values given in the caption of Fig. 7, and for the case of a constant mobility (thick curves), at 298 K and at (a) 3 V and (b) 10 V. The full and dashed thin curves have been obtained using Eq. (10) with the functions h_4 and h_2, respectively.

were obtained by carrying out 1D-ME calculations for a tenfold decreased intersite distance, thereby effectively switching off the field dependence of the mobility and recombination rate, and by taking $g(n)=1$. As discussed already in the introduction, the recombination rate is then quite uniform across the device, but decreases toward the electrodes in thin interfacial zones, and vanishes at the electrodes. With increasing voltage the thickness of these zones near the interfaces becomes smaller, as expected from the decrease in the relative contribution of the diffusion current to the total current with increasing voltage. The thin full and dashed curves give the recombination rate for various values of $\hat{\sigma}$ as obtained from Eq. (10) using the functions $h_k(F)$ with $k=4$ and 2, respectively.

The most striking result revealed by Fig. 5 is that, independent of the values of the k parameter considered, disorder leads to a strong confinement of the recombination profile to the center of the device. The effect is due to the density dependence of the mobility, as may be concluded from a comparison of the effects at 3 V and 10 V. At 3 V, the field in the device is quite modest, so that the density dependence of the mobility is the predominant effect. The confinement effect is already observed for $\hat{\sigma}=3$, and increases further with increasing disorder parameter. At 10 V a similar increase in the degree of confinement is observed. The effect may be understood as follows. In the device center, the electron and hole carrier densities and mobilities are equal by symmetry. However, at either side of the device center the carrier densities, and therefore also the mobilities, are strongly unbalanced. The mobility of the electrons and holes which have just passed the device center drops strongly, due to the disorder-induced carrier density dependence of the mobility, whereas the mobility of the other carrier increases. Therefore, most carriers which have just passed the device center will recombine quickly, well before arriving at the opposite electrode. We find that the introduction of injection barriers, leading to a reduction in the carrier concentration at the injecting interfaces to a 1% level, has almost no effect on the shape of the recombination profiles.

At 10 V and for the cases $\hat{\sigma}=3$ and 4 the recombination rate shows a local minimum in the device center, when using the function $h_4(F)$. This may be explained by considering the more important role played at high voltages by the field dependence of the mobility. The field is largest (most positive) in the device center. The carrier density in the device center needed for obtaining a certain current density can then be relatively small, as the mobility is field enhanced. In contrast, it is relatively large in the regions more close to the electrodes where the field shows a sign change toward negative values in the regions close to the electrodes. The recombination rate, which is proportional to the product of the electron and hole densities, is then relatively large in these regions more close to the electrodes, and smaller in the device center, as found already in Ref. 8 for the case of a material showing a Poole-Frenkel-type field-dependent mobility (but no carrier density dependence of the mobility). For higher disorder parameters the carrier density dependence of the mobility becomes more predominant, so that the recombination becomes more confined to the device center.

The stronger field dependence of the function h_2 as compared to h_4 leads in all cases considered to an enhanced recombination rate in the device center, where the field is largest. At 3 V, the different field dependence of the recombination rate as obtained when using the functions h_4 or h_2 is not yet very important. However, at 10 V the difference is much larger. It will thus be of practical interest to investigate using 3D-MC calculations how precisely the field dependence of the recombination rate should be described in systems with Gaussian disorder.

B. Asymmetric OLEDs

We have also studied the effects of Gaussian disorder in "asymmetric" devices, by varying $\mu_{0,e}$ while $\mu_{0,h}$ remains fixed. All other parameters are identical to those used above. Figure 6 shows the effect of varying the $\mu_{0,e}/\mu_{0,h}$ ratio on the enhancement of the current density in such devices, with $\hat{\sigma}$ equal to 3 and 6 and for $V=10$ V. The figure shows that the current density in devices with large disorder ($\hat{\sigma}=6$) is not only strongly enhanced with respect to the single-carrier current density when $\mu_{0,e}/\mu_{0,h}=1$, but already for quite small values of the electron mobility.

Figure 7 shows for such asymmetric OLEDs for various values of the ratio $\mu_{0,e}/\mu_{0,h}$ the normalized recombination rate profile at $V=10$ V, for $\hat{\sigma}$ equal to 3 [Fig. 7(a)] and 6 [Fig. 7(b)]. All other parameters used were the same as those given in the caption of Fig. 4. As is well known, the peak in the emission profile shifts to the cathode with decreasing $\mu_{0,e}/\mu_{0,h}$. It may be seen that with increasing disorder this asymmetry-induced shift becomes less pronounced, and that for strongly *asymmetric* devices high disorder gives rise to a

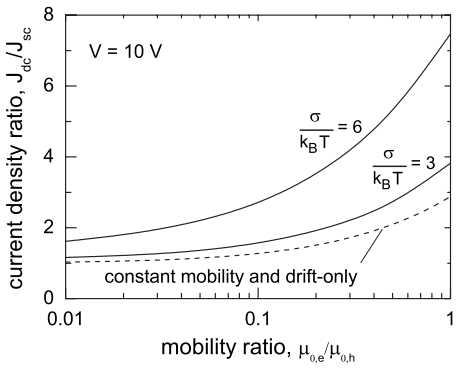

FIG. 6. Ratio of the current density in asymmetric double-carrier device and a single-carrier hole-only device, J_{dc}/J_{sc}, as a function of the ratio of the zero-field and zero-density electron mobilities for electrons and holes, $\mu_{0,e}/\mu_{0,h}$, for devices with a Gaussian DOS with $\hat{\sigma}$=3 and 6 (full curves), and for devices with a constant mobility using the Parmenter-Ruppel drift-only model (Ref. 5) (dashed curve). Apart from $\mu_{0,e}$, all other parameter values are the same as used in Fig. 4.

relatively *large* width of the profile. This may look somewhat paradoxical, as for *symmetric* devices high disorder gives rise to a relatively *small* width. This may be understood again by considering the effect of the density dependence of the mobility. Even for devices for which $\mu_{0,e} \ll \mu_{0,h}$, the electron mobility is close to the cathode, where the electron density is large, much larger than the hole mobility. Locally, the mobility asymmetry is thus reversed. The overall effect is a smaller effective asymmetry, resulting in a wider recombination profile with a peak which is shifted away from the cathode.

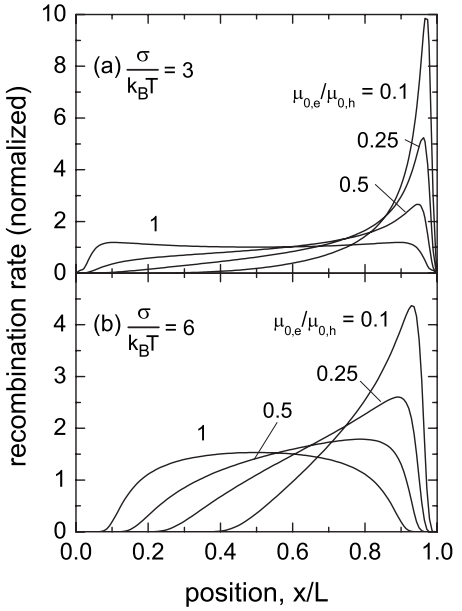

FIG. 7. Position dependence of the normalized recombination density in asymmetric 100 nm OLEDs for various values of $\mu_{0,e}/\mu_{0,h}$, for devices with a Gaussian DOS with (a) $\hat{\sigma}$=3 and (b) 6, at 10 V. Apart from $\mu_{0,e}$, all other parameter values are the same as used in Figs. 4 and 5 for studying symmetric devices.

IV. SUMMARY, CONCLUSIONS, AND OUTLOOK

In the first part of this paper a 1D-ME method has been developed for calculating the $J(V)$ curves and recombination profiles in sandwich-type devices in which the electron and hole DOS have a Gaussian shape. By the construction, in the zero-field limit the carrier density dependence of the mobility is equal to the results obtained within the EGDM and the recombination rate is consistent with the Langevin formula. An expression is given for the electron-hole pair generation rate.

The model may be used to provide a physically transparent interpretation of the numerical results obtained from 3D modeling of the mobility and recombination rate. Three examples of such applications of the model were presented. First, it was shown that the model predicts that the mobility may be written as a product of separate carrier-density-dependent and field-dependent factors, consistent with the empirical finding of such a factorizability in Ref. 11. Second, it was shown that the field dependence of the mobility as obtained from 3D-ME calculations can be understood when in our 1D model the intersite distance is taken to increase slightly with the disorder parameter $\hat{\sigma}$, instead of being equal to the actual average intersite distance. Physically, this reflects that the distance over which the mobility-determining hops take place increases with increasing $\hat{\sigma}$, as expected from percolation theory. Third, the model predicts that the field dependence of the recombination rate is enhanced with respect to the field dependence given by the Langevin formula, in agreement with a result obtained from 3D-MC calculations.[27] A simple expression is provided for describing this effect [Eq. (8)], containing a single parameter (k) which describes the relative weights of longitudinal and lateral hops.

In the second part of the paper, the method has been used to investigate how disorder affects the current density and recombination profile in single-layer OLEDs. A strong disorder-induced enhancement of the full (double-carrier) current density has been found as compared to the current density obtained in single-carrier devices based on the same material. Furthermore, in OLEDs with equal electron and hole mobility functions, the shape of the recombination profile becomes *more narrow*, i.e., more confined to the center of the layer with increasing disorder. The effect is already quite significant when $\hat{\sigma}$=6. In such a case, the light-outcoupling efficiency can be significantly enhanced as compared to the efficiency obtained in the case of a constant mobility and diffusion coefficient, for which the recombination profile is quite uniform across the device. In contrast, the recombination profile is found to become *wider* with increasing disorder in asymmetric OLEDs, with unequal electron and hole mobilities so that the recombination profile is located close to one of the electrodes. For voltages and layer thicknesses that are of practical interest, taking the enhanced field dependence of the recombination rate into account has been shown to be important. It will therefore be of interest to investigate the possible disorder, temperature, and charge-carrier density dependence of this effect in more detail using 3D Monte Carlo calculations.

We envisage that an important future application of the model would be the analysis of transport across organic-

organic interfaces. Within the scope of our model, ideally sharp interfaces are characterized by only two parameters, viz., the energy difference Δ between the transport levels in the two layers in the absence of a field, and the hopping distance, d, between the two adjacent layers. In the simplest case, with equal disorder parameters in both layers, Δ is equal to the HOMO or LUMO energy difference. However, even when the real average intersite distance at the interface is equal to the value a in the bulk of the layers, d is then not expected to be equal to the effective lattice parameter ζa, as the effective distance for "critical" (current density determining) hops across the interface is influenced by Δ. It would be of interest to investigate using 3D modeling to what extent such a description of the transport across interfaces indeed holds, and how d depends on Δ and σ. The model may then be applied to realistic multilayer OLEDs developed for, e.g., high-efficiency lighting applications.

The model may also be extended to include trap states, viz., by making use of the multiple-trap-and-release model.[37] It is then assumed that there is local thermal equilibrium between subpopulations of carriers residing in the Gaussian DOS and in the trap DOS, and that the transport is only due to the fraction of carriers residing in the Gaussian DOS. Giving a detailed discussion of this application is beyond the scope of this paper. We have successfully used the model to describe transport and recombination in single-layer blue-emitting OLEDs based on polyfluorene-based copolymers within which electron transport is influenced by traps.[38,39]

ACKNOWLEDGMENTS

The authors thank R. J. de Vries for useful comments and for carrying out supplementary calculations. This research was supported by NanoNed, a national nanotechnology program coordinated by the Dutch Ministry of Economic Affairs (contribution S.L.M.v.M) and by the European Community's Seventh Framework program (Grant No. 213708, AEVIOM, contribution R.C.).

APPENDIX A. TREATMENT OF CHARGE-CARRIER DIFFUSION WITHIN THE 1D-ME MODEL

Within the 1D-ME model developed in this paper the actual 3D system with Gaussian disorder is replaced by an effective 1D two-level system. Equations (1)–(4) describe the current density response to a local field. A disorder-parameter-dependent function $g(n,\hat{\sigma})$, deduced in Ref. 11 from the 3D-ME calculations, is used to describe the carrier density dependence of the mobility. In this appendix, we discuss to what extent the model appropriately describes charge-carrier diffusion.

The diffusion current density, which arises in the absence of an electric field as a result of the presence of a carrier density gradient, is within the 1D-ME model given by

$$J_{diff} = -\frac{e}{a^2}\frac{d[cg(n)]}{dx}\zeta a r_0 = -\mu_0 k_B T \frac{d[cg(n)]}{dx}, \quad \text{(A1)}$$

using $c=\zeta a^3 n$, Eqs. (1) and (4). From Eq. (1) and the definition of the diffusion coefficient, $D \equiv J_{diff}/[-e(dn/dx)]$, it follows that D is density dependent, as given by

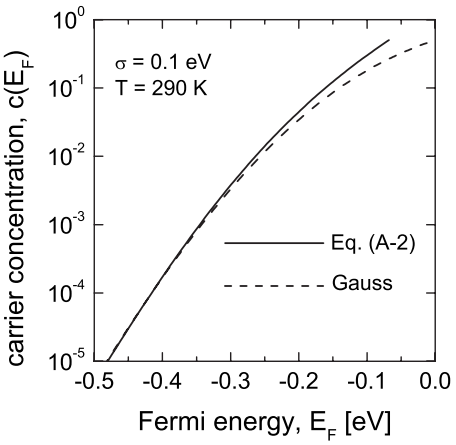

FIG. 8. Carrier concentration as a function of the Fermi energy, for a case with $\hat{\sigma}=4$ (with $\sigma=0.1$ eV and $T=290$ K), as used effectively in the 1D-ME model [full curve, Eq. (A2)] and as obtained for a Gaussian DOS (dashed curve).

$$D(n) = \frac{\mu_0 k_B T}{e}\frac{\dfrac{d[ng(n)]}{dx}}{\dfrac{dn}{dx}} = \frac{g(n)\mu_0 k_B T}{e}\left(1+\frac{n}{g}\frac{dg}{dn}\right). \quad \text{(A2)}$$

This expression may be compared with the generalized Einstein equation (GEE) for the diffusion coefficient, $D/\mu(n) = n/[e(dn/dE_F)]$, which follows from the requirement that in equilibrium the drift and diffusion currents between each pair of states are opposite (zero net current). This yields the following relation between the carrier density and the Fermi energy:

$$\frac{dE_F}{dn} = k_B T\left[\frac{1}{n}+\frac{1}{g(n)}\frac{dg(n)}{dn}\right]. \quad \text{(A3)}$$

It may be concluded that the 1D-ME model appropriately describes diffusion, including the enhancement of the diffusion coefficient as described by the GEE, if the DOS is taken to have a form which is consistent with Eq. (A3). In Fig. 8, an example is given. The full and dashed curves show the integrated carrier concentration as a function of the Fermi energy, as obtained using Eq. (A3) and as expected for a perfectly Gaussian DOS, respectively. For completeness, we give the mobility enhancement function used

$$g(n,\hat{\sigma}) = \exp\left[\frac{1}{2}(\hat{\sigma}^2-\hat{\sigma})\left(\frac{2n}{N_t}\right)^{\delta}\right] \quad \text{for} \quad n \le 0.1\times N_t, \quad \text{(A4)}$$

with $\delta = 2[\ln(\hat{\sigma}^2-\hat{\sigma})-\ln(\ln 4)]/\hat{\sigma}^2$. As motivated in Ref. 34, we take $g(n,\hat{\sigma}) = g(0.1\times N_t,\hat{\sigma})$ for $n > 0.1\times N_t$. The precise value of the cut-off density has no significant effect on the results presented in this paper. The figure shows that the two integrated carrier densities are quite close but not precisely equal. The effective DOS would be exactly Gaussian when

the mobility would be well described assuming a fixed transport level, and neglecting the effect of the final-state occupation probability on the hopping rates. The mobility enhancement function would then be given by $g(c) = \exp[E_{F,Gauss}(c)/(k_BT) + \hat{\sigma}^2/2]/c$ [see Ref. 30, Eq. (28)].

In principle, the proper effective $E_F(n)$ relationship derived above should be used when determining the carrier density boundary conditions corresponding to a certain injection barrier (see Sec. II A). We find that, in practice, this only has a significant effect on the current density when the voltage is small, so that the transport is predominantly due to charge-carrier diffusion.

APPENDIX B. REFINEMENT OF THE MODEL—HOPPING RATES AND RECOMBINATION AT HIGH ELECTRIC FIELDS

Figure 2 reveals that at high electric fields the field dependence of the mobility is not described well by Eq. (5). Due to the large field, the energy of most downstream nearest-neighbor states is lower than the energy of the initial state, so that the mobility-determining hops are no longer thermally activated.[11] In this subsection we will refine the 1D-ME model in such a way that for fields larger than a certain crossover field, F^*, the mobility is given by the exact expression for the mobility in the high-field limit, i.e.,

$$\mu_{1D}(c,F,\hat{\sigma}) = \frac{C_1 \nu_0 a}{F} = \frac{\sigma}{eaF} \times \mu^* \quad \text{for} \quad F > F^*. \tag{B1}$$

The first step in Eq. (B1) follows by writing the mobility as the ratio of the average velocity and the field, and the second step follows using the definition of μ^* given in Sec. II A.

Within the 1D-ME model, we interpret F^* as the field at which the effective thermal activation energy for forward hops becomes negative. In Fig. 9(a), the energy level structure at $F=F^*$ is shown. The effective activation energy for forward hops is equal to the *local* activation energy, $E_A(n) \equiv E_{tr} - E_0(n)$, minus a term $e\zeta aF/2$ [as shown in Fig. 1(b)], so that

$$F^* = 2\frac{E_A(n_i)}{e\zeta a}. \tag{B2}$$

On the other hand, it follows straightforwardly from the requirement of continuity of the mobility at $F=F^*$ that

$$F^* \cong [C_2\hat{\sigma}^2 + \ln(\zeta\hat{\sigma}) - \ln g(n,\hat{\sigma})] \times \frac{2k_BT}{e\zeta a}, \tag{B3}$$

using that to an excellent approximation $f(\hat{F}^*) \approx \exp(\hat{F}*)/(2\hat{F}^*)$. E_A is thus given by

$$E_A(n) \cong [C_2\hat{\sigma}^2 + \ln(\zeta\hat{\sigma}) - \ln g(n,\hat{\sigma})] \times k_BT. \tag{B4}$$

In order to avoid unnecessary notational complexity, the dependence of E_A on T, σ and the site density $N_t = a^{-3}$ have not been indicated. As $E_A(n)$ decreases with increasing carrier density, F^* is predicted to decrease with increasing carrier density. Figure 2 shows that the $\hat{\sigma}$ and carrier density dependence of the field at which the regime change takes place is quite well predicted by the 1D-ME model. In view of the simplicity of the 1D model, it is not surprising that the predicted effect of the regime change on the mobility is more abrupt than in the full 3D model.

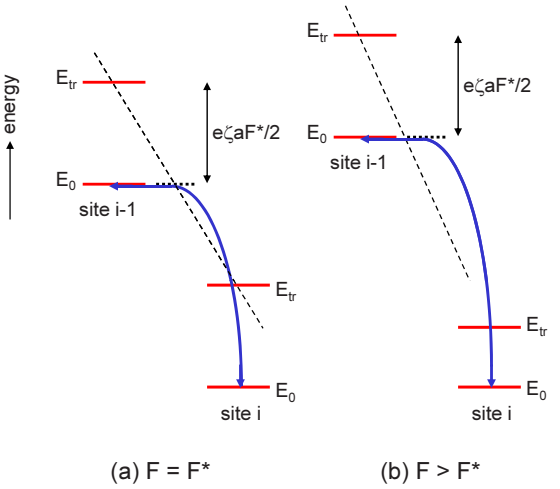

FIG. 9. (Color online) Schematic view of the hopping process at (a) $F=F^*$, for the special case in which the carrier concentration is the same at both sites and (b) $F>F^*$, for the general case of different carrier concentrations at both sites. At each site the effective initial state level E_0 and the transport level E_{tr} are shown. The field in interval i is proportional to the slope of the thin dashed line. The thick horizontal dashed line in between both sites indicates the effective thermal activation level. In both cases, only hops from site i to site $i-1$ are thermally activated.

We now consider a device with a nonuniform carrier density and field, and focus on transport across an interval i. For fields $F_i > F_i^*$ [see Fig. 9(b)] we assume that the rate of downhill hops is independent of the final-state energy and equal to the rate at $F=F^*$. The effective activation energy is thus assumed to be determined by the position of the thick dashed energy level indicated in Fig. 9(b) in between sites $i-1$ and i. This is consistent with the assumption made within the framework of the Millar-Abrahams theory concerning the dependence of the hopping probability on the difference between the initial and final state energies.[40] The forward hopping rate is then given by

$$r_i^+ = r_{0,i-1} \exp\left(\frac{E_{A,i-1}(0)}{k_BT}\right) \quad \text{if} \quad F_i > F_i^*. \tag{B5}$$

By construction, this expression yields the high-field mobility given by Eq. (B1). Assuming that also for the backward hops the effective activation energy is determined by the dashed energy level in Fig. 9(b), the backward hopping rate is given by

$$r_i^- = r_{0,i} \exp\left(\frac{-e\zeta a F_i + E_{A,i-1}(n_{i-1}) - E_{A,i}(n_i) + E_{A,i}(0)}{k_B T}\right) \quad \text{if} \quad F_i > F_i^*. \tag{B6}$$

In devices with a homogeneous large field, the backward hopping rate is negligible. However, in inhomogeneous systems, in particular at internal (organic-organic) interfaces, Eq. (B6) is relevant.

In a field $F > F^*$, the field dependence of the recombination rate is different from the functions h_k given by Eq. (8). The effect of backward and lateral hops can then be neglected, and the average velocity of the carriers is independent of the field. Therefore, also the recombination rate is then independent of the field: $h_k(F) \approx \exp(\hat{F}^*)/(2+k)$. As now $f(F) \approx (1/2)\exp(\hat{F}^*)/\hat{F}$, one finds that $h_k(F)/f(F) \approx [2/(2+k)]\hat{F}$. It may be easily verified that the same linear dependence on F is also obtained when extrapolating the h/f ratio for fields below F^*. For the case considered in Fig. 6, $F^* \approx 4 \times 10^8$ V/m at 300 K, i.e., outside the field range given in Fig. 6. However, it is evident from the figure that the linear dependence of h/f on F sets in at fields already well below F^*.

[1] B. W. D'Andrade and S. R. Forrest, Adv. Mater. **16**, 1585 (2004).
[2] K. Walzer, B. Maennig, M. Pfeiffer, and K. Leo, Chem. Rev. (Washington, D.C.) **107**, 1233 (2007).
[3] F. So, J. Kido, and P. Burrows, MRS Bull. **33**, 663 (2008).
[4] K. A. Neyts, J. Opt. Soc. Am. A Opt. Image Sci. Vis **15**, 962 (1998); M.-H. Lu and J. C. Sturm, J. Appl. Phys. **91**, 595 (2002); J. M. Leger, S. A. Carter, B. Ruhstaller, H.-G. Nothofer, U. Scherf, H. Tillman, and H.-H. Hörhold, Phys. Rev. B **68**, 054209 (2003).
[5] R. H. Parmenter and W. Ruppel, J. Appl. Phys. **30**, 1548 (1959).
[6] M. Pope and C. E. Svenberg, *Electronic Processes in Organic Crystals and Polymers* (Oxford University Press, New York, 1999).
[7] F. Neumann, Y. A. Genenko, R. Schmechel, and H. von Seggern, Synth. Met. **150**, 291 (2005).
[8] B. K. Crone, P. S. Davids, I. H. Campbell, and D. K. Smith, J. Appl. Phys. **84**, 833 (1998); S. J. Konezny, D. L. Smith, M. E. Galvin, and L. J. Rothberg, *ibid.* **99**, 064509 (2006).
[9] H. Bässler, Phys. Status Solidi B **175**, 15 (1993).
[10] Y. Roichman, Y. Preezant, and N. Tessler, Phys. Status Solidi A **201**, 1246 (2004).
[11] W. F. Pasveer, J. Cottaar, C. Tanase, R. Coehoorn, P. A. Bobbert, P. W. M. Blom, D. M. de Leeuw, and M. A. J. Michels, Phys. Rev. Lett. **94**, 206601 (2005).
[12] J. Zhou, Y. C. Zhou, J. M. Zhao, C. Q. Wu, X. M. Ding, and X. Y. Hou, Phys. Rev. B **75**, 153201 (2007).
[13] S. L. M. van Mensfoort, S. I. E. Vulto, R. A. J. Janssen, and R. Coehoorn, Phys. Rev. B **78**, 085208 (2008).
[14] P. S. Davids, A. S. Saxena, and D. L. Smith, J. Appl. Phys. **78**, 4244 (1995).
[15] P. W. M. Blom, M. J. M. de Jong, and S. Breedijk, Appl. Phys. Lett. **71**, 930 (1997).
[16] J. Shen and J. Yang, J. Appl. Phys. **83**, 7706 (1998).
[17] J. Staudigel, M. Stössel, F. Steuber, and J. Simmerer, J. Appl. Phys. **86**, 3895 (1999).
[18] G. G. Malliaras and J. C. Scott, J. Appl. Phys. **83**, 5399 (1998); **85**, 7426 (1999).
[19] J. C. Scott, P. J. Brock, J. R. Salam, S. Ramos, G. G. Malliaras, S. A. Carter, and L. Bozano, Synth. Met. **111-112**, 289 (2000).
[20] P. W. M. Blom and M. C. J. M. Vissenberg, Mater. Sci. Eng. **27**, 53 (2000).
[21] I. H. Campbell and D. L. Smith, *Solid State Physics: Advances in Research and Applications* (Academic Press, San Diego, 2001), Vol. 55, pp. 1–117.
[22] W. Brütting, S. Berleb, and A. G. Mückl, Org. Electron. **2**, 1 (2001).
[23] A. B. Walker, A. Kambili, and S. J. Martin, J. Phys.: Condens. Matter **14**, 9825 (2002).
[24] B. Ruhstaller, T. Beierlein, H. Riel, S. Karg, J. C. Scott, and W. Riess, IEEE J. Sel. Top. Quantum Electron. **9**, 723 (2003).
[25] H. Houili, E. Tutiš, H. Lütjens, M. N. Bussac, and L. Zuppiroli, Comput. Phys. Commun. **156**, 108 (2003); D. Berner, H. Houili, W. Leo, and L. Zuppiroli, Phys. Status Solidi A **202**, 9 (2004).
[26] Z. G. Yu, D. L. Smith, A. Saxena, R. L. Martin, and A. R. Bishop, Phys. Rev. B **63**, 085202 (2001); E. Tutiš, I. Batistić, and D. Berner, *ibid.* **70**, 161202(R) (2004); K. D. Meisel, W. F. Pasveer, J. Cottaar, C. Tanase, R. Coehoorn, P. A. Bobbert, P. W. M. Blom, D. M. de Leeuw, and M. A. J. Michels, Phys. Status Solidi C **3**, 267 (2006).
[27] U. Albrecht and H. Bässler, Chem. Phys. Lett. **235**, 389 (1995); Phys. Status Solidi B **191**, 455 (1995).
[28] C. Groves and N. C. Greenham, Phys. Rev. B **78**, 155205 (2008).
[29] D. Monroe, Phys. Rev. Lett. **54**, 146 (1985).
[30] R. Coehoorn, W. F. Pasveer, P. A. Bobbert, and M. A. J. Michels, Phys. Rev. B **72**, 155206 (2005), and references therein.
[31] Y. Roichman and N. Tessler, Appl. Phys. Lett. **80**, 1948 (2002).
[32] W. F. Pasveer, Ph.D. thesis, Eindhoven University of Technology, 2005.
[33] J. J. M. van der Holst, M. A. Uijttewaal, B. Ramachandhran, R. Coehoorn, P. A. Bobbert, G. A. de Wijs, and R. A. de Groot, Phys. Rev. B **79**, 085203 (2009).
[34] S. L. M. van Mensfoort and R. Coehoorn, Phys. Rev. B **78**, 085207 (2008).
[35] P. W. M. Blom, M. J. M. de Jong, and C. T. H. F. Liedenbaum, Polym. Adv. Technol. **9**, 390 (1998).
[36] B. G. Martin, J. Appl. Phys. **75**, 4539 (1994).
[37] D. C. Hoesterey and G. M. Letson, J. Phys. Chem. Solids **24**, 1609 (1963).
[38] S. Harkema, R. A. H. J. Kicken, B. M. W. Langeveld, S. L. M. van Mensfoort, M. M. de Kok, and R. Coehoorn, (unpublished).
[39] S. L. M. van Mensfoort, Ph.D. thesis, Eindhoven University of Technology, 2009.
[40] A. Miller and E. Abrahams, Phys. Rev. **120**, 745 (1960).